Bull. Mater. Sci. (2023)46:145
https://doi.org/10.1007/s12034-023-02977-5

Highly efficient dye-sensitized solar cells with TiO_2-coated silver nanowire-incorporated tri-layered photoanode

H K H D KANKANAMGE[1], J M K W KUMARI[1,3], M A K L DISSANAYAKE[1,3], G K R SENADEERA[1,3,4], B S DASSANAYAKE[1,2] and H C S PERERA[1,*]

[1]Postgraduate Institute of Science, University of Peradeniya, Peradeniya 20400, Sri Lanka
[2]Department of Physics, Faculty of Science, University of Peradeniya, Peradeniya 20400, Sri Lanka
[3]National Institute of Fundamental Studies, Kandy 20000, Sri Lanka
[4]Department of Physics, The Open University of Sri Lanka, Nugegoda 11222, Sri Lanka
*Author for correspondence (chanip@sci.pdn.ac.lk)

MS received 21 October 2022; accepted 21 March 2023

Abstract. This study is about investigating the effect of adding TiO_2-coated silver nanowires into a tri-layered photoanode of dye-sensitized solar cells (DSSCs) to improve the photovoltaic performance. Face-centred cubic silver nanowires (AgNWs) were synthesized via a rapid, scalable and green pathway method. The average length and diameter of AgNWs were 5 μm and 70 nm, respectively. AgNWs were coated with titanium dioxide (TiO_2) using 2-mercaptoethanol as the binder. AgNW@TiO_2 core-shell structure was formed by the hydrothermal method and the average diameter of the coated TiO_2 was observed to be 14 nm. TiO_2 shell showed anatase phase, which was a significant advantage for higher dye absorbance leading to a higher power conversion efficiency (PCE). The PCE for a DSSC with single-layered TiO_2 photoanode increased from 6.70 to 8.87% due to AgNW@TiO_2 core-shell structured photoanode, reflecting a 32.3% enhancement. The PCE for a DSSC with tri-layered AgNWs@TiO_2 core-shell structured photoanode was 10.5% showing an impressive enhancement of 49.6% compared to the DSSC with a pure tri-layered TiO_2 photoanode. TiO_2 shell appears to act as a protective shell around AgNWs by both resisting redox chemical corrosion of Ag by iodide ions in the electrolyte and increasing the thermal stability of AgNWs against annealing at high temperatures. Further, TiO_2-coated AgNWs facilitate increased photoelectron generation by plasmonic effect, reduce the recombination and enhance the electron lifetime while providing a direct pathway for excited electrons leading to a significant improvement in the PCE of DSSC.

Keywords. Dye-sensitized solar cells; efficiency enhancement; TiO_2-coated silver nanowires; tri-layered photoanode; plasmonics effect.

1. Introduction

The first dye-sensitized solar cell (DSSC) was reported by O'Regan and Grätzel [1]. DSSCs are considered a class of potential alternative devices for p–n junction silicon solar cells [2,3]. Researchers pay increased attention to DSSCs because they are inexpensive, require a simple fabrication process, have adaptable cell design and have moderate efficiency [2]. The DSSC structure consists of an anode, a cathode and an electrolyte [4,5]. The anode consists of a wide bandgap semiconductor material coated on a transparent conducting oxide, and a dye which can absorb light photons in the visible range wavelengths. The cathode or the counter electrode is made up of a catalyst deposited on a transparent conducting oxide. Platinum is most commonly used as the counter electrode material and the electrolyte acts as the connector between the anode and the cathode [2,5].

The PCE of a DSSC can be enhanced by increasing the thickness of the TiO_2 substrate, which leads to high dye absorption. However, recombination of electrons increases with increasing photoanode thickness causing higher dark currents [2,5]. For regular liquid electrolyte DSSC, the optimized photoanode thickness is around 12 μm. Metal nanostructures (MNSs) can be introduced into the photoanode, which increases the light absorption and scattering cross-section via generating surface plasmons (SPs) that either resonate locally (i.e., localized surface plasmonic resonance or LSPR) or propagates along the metal/dielectric surface (surface plasmon polariton or SPP) causing more efficient photoelectron generation and charge separation, which enhances power conversion efficiency (PCE) of the DSSC [2,5–8]. Here, the surface plasmon resonance (SPR) is the charge density oscillation for a specific EM wavelength (light), which is unique to a given size, shape and material of the plasmonic nanostructure, and the

Published online: 14 July 2023

surrounding dielectric environment [5,7,9,10]. SPR from MNSs can offer particularly remarkable control over the optical field, making it possible to utilize light absorption enhancement in thin-film solar cells. If the MNS dimensions are comparable to or smaller than the specific light wavelength that is used to excite the SPs in the MNS, the generated SPs are localized to the MNS and it is called LSPR [4]. Therefore, adding MNSs to TiO_2-based photoanode can enhance the PCE due to the non-radiative coupling of incoming photons with TiO_2 conduction electrons [9–13].

Quantum confinement can be achieved if the size of the nanostructure is reduced below the Bohr exciton radius of the bulk material of the nanostructure. When a nanostructure achieves quantum confinement, the random moving electrons in the bulk material are restricted to discrete energy levels [8].There are different types of quantum confined MNSs such as zero dimension (0-D) (electron movement is restricted in all three dimensions) and one dimension (1-D), etc. and we can add the above quantum-confined MNSs into the photoanode to increase the PCE [5,9,11–14]. However, there are limitations such as adding 0-D structures, like metal nanoparticles (MNPs) or quantum dots into photoanode increases the recombination probability of electrons due to short electron diffusion length in the order of 7–30 μm, which increases the recombination probability of electrons [2,3]. To produce optically thick photoanodes, scientists have tried to reduce the recombination and increase electron charge transportation by introducing alternative nanostructures like 1-D structures (nanofibre, nanowire, nanotube and nanorods) and they can improve the electron transfer by providing a direct conduction pathway for excited electron [5,9]. Further, if devised carefully, photoexcited electrons can be transferred to the unoccupied conduction states of TiO_2 to improve the photo-current of DSSC. To enhance the PCE of DSSC by adding MNSs into photoanode, the chosen MNSs must have high electron density, excellent SPR, better electron transfer and excellent absorption of the dye. Silver (Ag) is one of the noble materials with the characteristics stated above. We have reported improvement in light absorption of the dye via plasmon resonance by incorporating Ag nanoparticles (NPs) [15], and Jeong *et al* [16] have reported a 25% improvement of PCE by introducing Ag NPs into photoanode. Ag nanowires (AgNWs) have been identified to improve PCE owing to high electron density, optical plasmonic and catalyst property, and by reducing the recombination of electrons through providing a direct pathway to excited electrons [2,5–18]. However, the incorporated AgNWs must be able to withstand high thermal energy because the annealing process for the TiO_2-based photoanode is above 450C [8,18]. As a solution, the surface of AgNWs can be coated with TiO_2 NPs, which have high thermal stability. Chen *et al* [19] have prepared TiO_2-coated AgNWs (AgNWs@TiO_2) via dispersing AgNWs in TiO_2 gel for 24 h (h). The constructed DSSC with AgNWs@TiO_2-incorporated photoanode and N3 dye showed 4% PCE, which gave a twofold enhancement of the PCE compared to reference DSSC. Jang *et al* [4] have reported 5.56% PCE, which was a 10% improvement of PCE compared to the reference cell. They have used 2-mercaptoethanol to bind TiO_2 onto the AgNW surface [4].

In this study, we focus on fabricating AgNWs and coating TiO_2 on the surface of AgNWs by using 2-mercaptoethanol as the chemical binder. Synthesized material was used to modify the tri-layered photoanode of the DSSC. To the best of our knowledge, this is the first report of using TiO_2-coated AgNWs in a tri-layered TiO_2 photoanode and using it in a DSSC to obtain the highest efficiency of 10.5% reported so far for a DSSC with a tri-layered photoanode.

2. Experimental

2.1 *Materials*

Silver nitrate ($AgNO_3$, Sigma-Aldrich, S6506, 99.0%), polyvinyl pyrrolidone (PVP, Mw = 44,000, BOH Laboratories), glycerol ($C_3H_8O_3$, Sigma-Aldrich, G8773, 99%), sodium chloride (NaCl, Sigma-Aldrich, 99.5%), 2-mercaptoethanol ($HSCH_2CH_2OH$, Sigma-Aldrich, M6250, 99%,), ethanol (C_2H_5OH, Sigma-Aldrich, 208821.321, 99%,), titanium(IV) butoxide (TBOT) ($C_{16}H_{36}O_4Ti$, Sigma-Aldrich, 244112, 99%), titanium dioxide P90 powder (Evonik), titanium dioxide P25 powder (Degussa), nitric acid (HNO_3, Sigma-Aldrich, 96.6%), Triton-X ($C_{14}H_{22}O(C_2H_4O)_{n\ (n=9-10)}$), Sigma-Aldrich, 99%, X100-500 ml, 99.0%), polyethylene glycol-2000 (PEG-2000) ($C_{133}H_{267}N_2O_{55}P$, Sigma-Aldrich, 99%), Ethylene carbonate (EC, Fluka, 03519, 99%), acetonitrile (CH_3CN, Sigma-Aldrich, 34851, 99.9%), tetraproplyammonium iodide (PrNI, Sigma-Aldrich, 235954, 99%), ruthenium dye N719 [RuL2(NCS)2:2TBA (L = 2,2′-bipyridyl-4, 4′-dicarboxylic acid, Solaronix), and iodine (I_2, Sigma-Aldrich, 57650, 99%) were used as received without any further purification. The deionized (DI) water was used from the Millipore system.

2.2 *Synthesis of AgNWs*

First, 1.5 g of PVP was added to 47.5 ml of glycerol solute. The solution was gently heated up to 80°C while stirring until all the PVP were completely dissolved. Then, the solution was cooled down to room temperature. Next, 0.125 ml of 5 mM NaCl, 0.395 g of $AgNO_3$, and additional 2.5 ml glycerol were added to the previously prepared solution. After that, the solution was heated up to 210°C by keeping an 8°C min^{-1} temperature gradient. Then the solution was cooled down to room temperature [20]. After the reaction, the mixture was centrifuged at 6000 rounds per minute (rpm) for 30 min (min) and washed with absolute

ethanol. The prepared nanowires were re-dispersed in ethanol for further characterization.

2.3 *Functionalizing the surface of AgNWs*

To functionalize the surface of AgNWs, first, 2-mercaptoethanol solution was prepared by adding 3.42 µl 2-mercaptoethanol into 10 ml ethanol. The prepared 2-mercaptoethanol solution was added dropwise into a 10 ml AgNWs dispersion, stirring under 150 rpm for 2 h. After that, the solution was ultrasonicated for 5 min and left to rest for 2 h. This cycle was carried out for 12 h. Finally, the solution was centrifuged at 4000 rpm for 10 min and the precipitate was re-dispersed in ethanol [4].

2.4 *Fabricating core-shell structure*

To prepare the TiO_2-coated core-shell structured AgNWs, first, 1.72 µl TBOT and 4 ml DI water were added into 10 ml ethanol. Then, the prepared solution was added dropwise into the functionalized AgNWs. The solution was stirred for another 20 min before transferring solution into a 100 ml Teflon-lined autoclave. The hydrothermal synthesis was conducted at 120°C for 12 h. Finally, the precipitate was centrifuged at 3500 rpm for 15 min and stored in ethanol [21].

2.5 *Fabricating of DSSCs*

2.5a *Fabricating compact layer:* A 0.25 mg of P-90 was measured and 0.1 M of HNO_3 was added dropwise into the mortar and ground for 20 min until the cream paste appeared. The paste was later, spin-coated on a fluorine-doped tin oxide (FTO)-coated glass at 3000 rpm [2].

2.5b *Fabricating photoanode:* A 0.25 mg of P-25 was measured and 0.1 M HNO_3 was dropwise added into the mortar. A 1 mg of Triton-X was added into the mixture and ground for 10 min. After that, 1 mg of PEG-2000 was added to the remaining paste. The mixture was ground for 20 min until white cream appeared [2].

2.5c *Fabricating AgNWs@TiO_2 photoanode:* A 0.25 mg of TiO_2 was measured and 0.1 M HNO_3 was added dropwise into the mortar and ground for 10 min. Previously optimized AgNWs@TiO_2 was added into the mortar and ground for another 10 min. After that, 1 mg of Triton-X and 1 mg of PEG-2000 were added simultaneously. The mixture was ground for 20 min until the white cream paste appeared.

2.5d *Fabricating tri-layers DSSC:* First, the P-90 compact layer was spin-coated on an FTO-coated glass. Then, the glass was sintered at 450°C for 45 min by keeping the temperature gradient at 20°C min^{-1}. P-25 paste was applied on the compact layer by Doctor Blade method at 80°C and again sintering at 450°C for 45 min. After that, AgNWs@TiO_2 photoanode (which was optimized using single-layer DSSC) was applied using the Doctor Blade method on the P-25 layer and again sintered at 450°C for 45 min. The final P-25 layer was applied using the doctor blade technique on the AgNWs@TiO_2 layer by keeping AgNWs@TiO_2-incorporated layer sandwich between two P25 layers. Subsequently, the films were sintered at 450°C for 45 min and allowed to cool down to room temperature. The effective cell area was kept as 0.25 cm^{-2}. Finally, the films were dipped in 0.3 mM ethanolic N719 ruthenium dye solution for 24 h at room temperature, and the films were washed gently with ethanol and were dried in air before cell assembly [5,22,23]. The schematic diagram of the prepared device is shown in figure 1b, and the corresponding energy level diagram for the device is depicted in figure 1c.

2.5e *Preparation of electrolyte:* A 3.6 g of molten ethylene carbonate (EC) was added to a volumetric flask. A 1 ml of acetonitrile was added into molten EC and then, 0.738 g of tetrapropylammonium iodide (Pr_4NI) was added into the previous mixture. Finally, 0.060 g of I_2 was added into a volumetric flask and stirred for 24 h [2].

2.6 *Characterization methods*

2.6a *Scanning electron microscope and transmission electron microscope:* Scanning electron microscope (SEM, (HE Hitachi SU6600 SEM, and Zeiss EVO LS15) and transmission electron microscope (TEM, JEOL JEM-2100 (Japan)) were used to study the dimension and morphology of the Ag NWs and core-shell structured AgNWs@TiO_2 and cross-section of the completely prepared cell and its reference cell. TEM was used to study the coating of the TiO_2 on the surface of the AgNWs [4].

2.6b *UV-–visible spectrum:* UV–visible spectrum for AgNWs, functionalized AgNWs and TiO_2-coated AgNWs were obtained using a Shimadzu UV-1800 spectrometer to study the optical absorption. The standard protocol was used to analyse the samples [2,4,5].

2.6c *X-ray diffractometer:* X-ray diffractometer (XRD, Bruker D8 Advanced Eco) was used to analyse the crystal structures of photoanode and the AgNWs@TiO_2 material. A photoanode was prepared using the usual method from that a powder sample was collected. And then XRD analysis was carried out.

2.6d *X-ray photoelectron spectroscopy:* X-ray photoelectron spectroscopy (XPS, Thermo Scientific TM

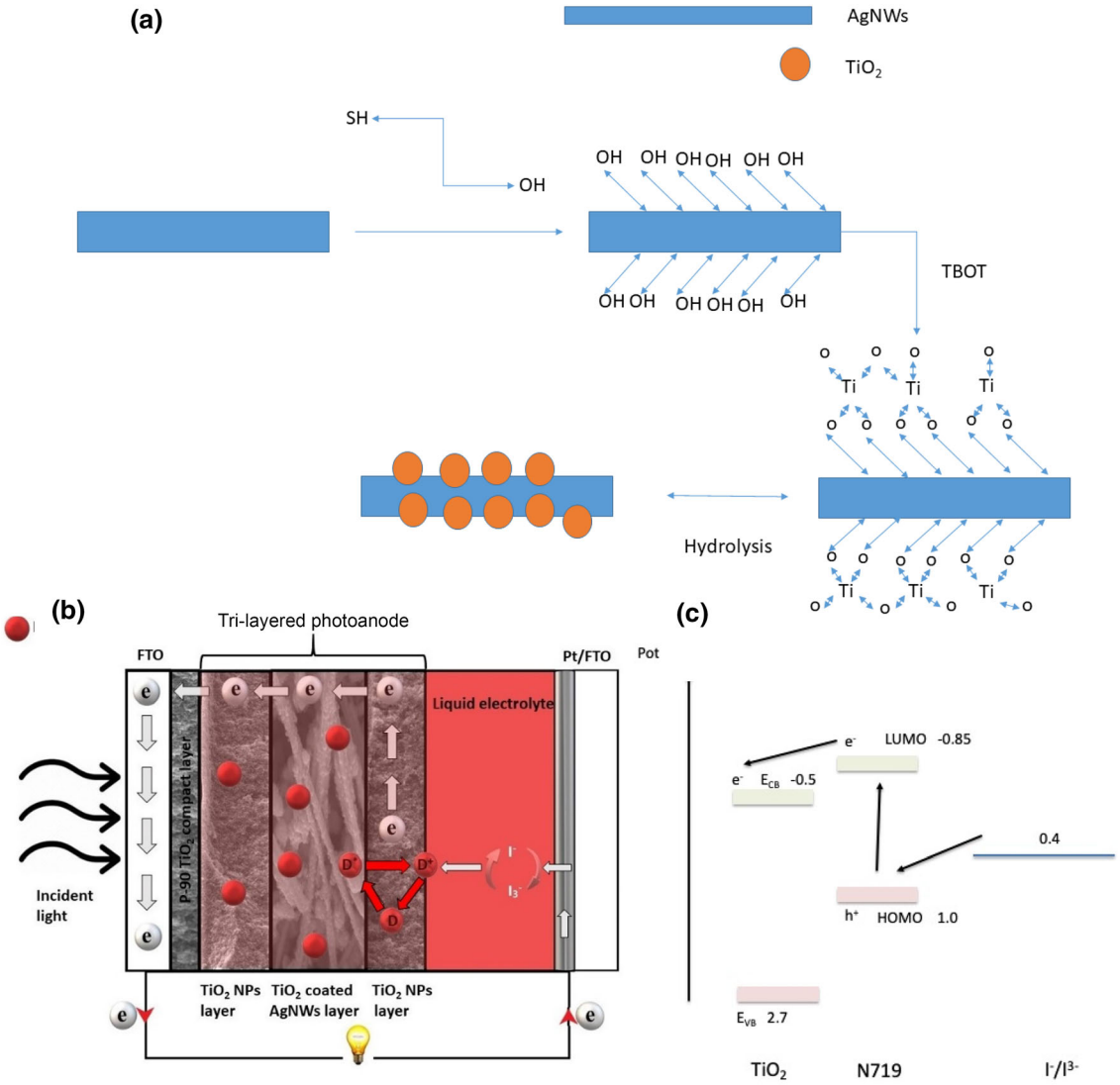

Figure 1. Schematic diagram of the (**a**) synthesis of AgNWs@TiO_2 using 2-mercaptoethanol chemical binder, (**b**) proposed device structure with electron transfer mechanism, and (**c**) corresponding energy band diagram.

ESCALAB Xi+) analysis was conducted to study the chemical composition of AgNWs@TiO_2 and the coating of Ag-TiO_2 [4]. In order to analyse the chemical composition, prepared AgNWs@TiO_2 and P25 mixture was done by doctor blade method on normal glass and carried out XPS analysis on standard conditions [4].

2.6e *J–V characterization:* *J–V* measurement was conducted by the Autolab Metrohm PGSTAT 128N coupled with sunlight illuminating at 100 mW cm^{-2} (AM 1.5). A xenon 500 W lamp with 1.5 filters was used as a solar simulator to obtain the above intensity. The measurement was conducted by following procedure of *J–V* measurement for a 0.25 cm^{-2} cell area [2,5].

2.6f *Dye loading:* Dye loading test was conducted by the Shimadzu UV-1800 spectrometer. The first concentration series of dye was prepared by using the original dye. The standard graph of absorbance amount *vs.* concentration was plotted under 535 nm wavelength and an unknown dye was inserted and particular absorbance was detected according to that particular concentration was matched. Finally, the absorbed dye amount was calculated by using equation (1) [2].

$$N(\text{mol}) = (C_1 - C_2) \times V \tag{1}$$

2.6g *Incident monochromatic light current conversion efficiency:* The characterization was done using the solar cell under the monochromatic condition. The experimental setup consisted of a monochromatic light source from a Bentham PVE300 unit coupled with a TMC 300 monochromator-based incident monochromatic light current conversion efficiency (IPCE) unit. The

monochromatic light source is a 150 W arc lamp. The wavelength was changed from 385 to 800 nm and the corresponding photocurrent of the solar cells and calibrated photodiode were observed. A calibrated Si photodetector was used as the reference [2,5].

2.6h *Electrochemical impedance spectroscopy:* Electrochemical impedance spectroscopy (EIS) was measured on DSSCs using Metrohm Potentiostat/Galvanostat PGSTAT 123N with Frequency Response Analyzer (FRA) 32M covering the 1 MHz to 0.01 Hz frequency. The measurements were carried out under the 1000 W m^{-2} using the same solar simulator as *J–V* measurements [2,5].

3. Results and discussion

3.1 *Formation of AgNWs*

Several factors depend on the formation of AgNWs such as the reducing agent used, reaction temperature, and amount of water in the reaction system, metal halide control agent, and the capping agent, etc. To synthesis AgNWs, glycerol was used as the reaction medium as well as the reducing agent to reduce Ag^+ ions into Ag atoms. Glycerol has higher polarity and adding a little amount of water further improves the polarity of the reaction medium, which helps to improve the solubility of Ag^+ ions. NaCl was used as the catalyst for the synthesis of AgNWs with high production yield [21]. PVP was used as a capping agent, which chemically interacts with the surface of Ag by Ag–O bonds and prevents the aggregation of small AgNPs [5,20,24].

Initially, when the solution temperature is gradually increased, the elemental Ag atoms are formed by reducing Ag^+ ions with glycerol in the presence of Cl^-. These formed Ag atoms are joined together to form Ag crystals with different shapes such as twinned and single-crystals. As the reaction continued, by further raising the temperature, the formation of the large shapes of Ag occurred by the Ostwald ripening process [5,20–25]. These larger AgNPs grow into rod-shaped nanostructures depending on strong interaction between the (100) face of Ag metal and PVP capping agent. Finally, AgNWs can be obtained due to the rapid growth of the ends ((111) facets) of the Ag nanorods. In this reaction process, AgNPs with different shapes and morphologies may be present due to the different growth velocities of crystal planes of Ag seeds [21].

The high concentration of Cl^- ions in the solution not only help electrostatic stabilization of the nanoparticles but also reduces the free Ag^+ ions in the solution by forming AgCl and later slowly releases the Ag^+ helping the formation of stable multiple twinned Ag seeds and effectively favouring anisotropic growth of AgNWs. When multiple twinned particles are formed, Ag atoms are attracted to the (111) plane as it has the highest surface energy during the Ostwald ripening process and crystalizes along the same plane. Selective binding of PVP to (100) plane prevents nucleation of Ag atoms at this plane forming elongating the twin seed forming a 1-dimensional nanostructure along (111) facets [21], which can be confirmed by XRD analysis [5,24]. Since multiple twinned particles have defects that provide high-energy sites, they are more susceptible to oxidative etching. Na^+ helps remove oxygen from the solution blocking the twinned particles from dissolving via oxidative etching and scavenging adsorbed atomic oxygen from the surface of the silver seeds [24,25].

3.2 *Formation of TiO_2-coated AgNWs*

Synthesized AgNWs were functionalized with 2-mercaptoethanol prior TiO_2 coating on the surface of the AgNWs. 2-Mercaptoethanol consists of thiol groups and hydroxyl groups. The thiol group interacts with the surface of AgNWs by displacing the PVP capping agent, and the hydroxyl group interacts with the added TBOT. This will help to obtain a uniform coating of TiO_2 throughout the surfaces of AgNWs [6]. The schematic diagram of the synthesis AgNWs@TiO_2 is represented in figure 1a.

3.3 *SEM and TEM images of synthesized AgNWs and AgNW@TiO_2*

SEM images of synthesized AgNWs@TiO_2 are shown in figure 2a. It can be clearly seen that the small TiO_2 nanoparticles are uniformly deposited on the surfaces of AgNWs. The diameter of synthesized AgNWs@TiO_2 are in the range of 40–100 nm. Also, it is observed that the particles with different sizes and shapes are present with the AgNWs@TiO_2 those may be due to agglomeration of TiO_2 nanoparticles or unreacted AgNPs as mentioned above. To get more information about the structure of AgNWs and AgNWs@TiO_2, TEM images were taken for the synthesized samples. The TEM image of AgNWs and AgNWs@TiO_2 are shown in figure 2d and e, respectively.

According to figure 2d, the diameter of AgNW is around 40–100 nm. Figure 2e shows that the AgNWs are coated by a uniform layer of TiO_2 nanoparticles with a thickness around 14 nm. The coating thickness of TiO_2 can be controlled with the concentration of the titania precursors. To study this, the concentration of the used TBOT was varied to 1.74, 3.48 and 5.22 mM to get a better core-shell structure. The surface morphologies of each concentration are represented in SEM images as figure 2a, b and c. As shown in the images, the best coating was for the 1.74 mM concentrated TBOT added system. A similar study has been reported by Ramasamy *et al* [24], where an increase of the TiO_2 shell thickness from 10 to 85 nm is reported by varying the concentration of TBOT from 4.5 to 6.5 μM.

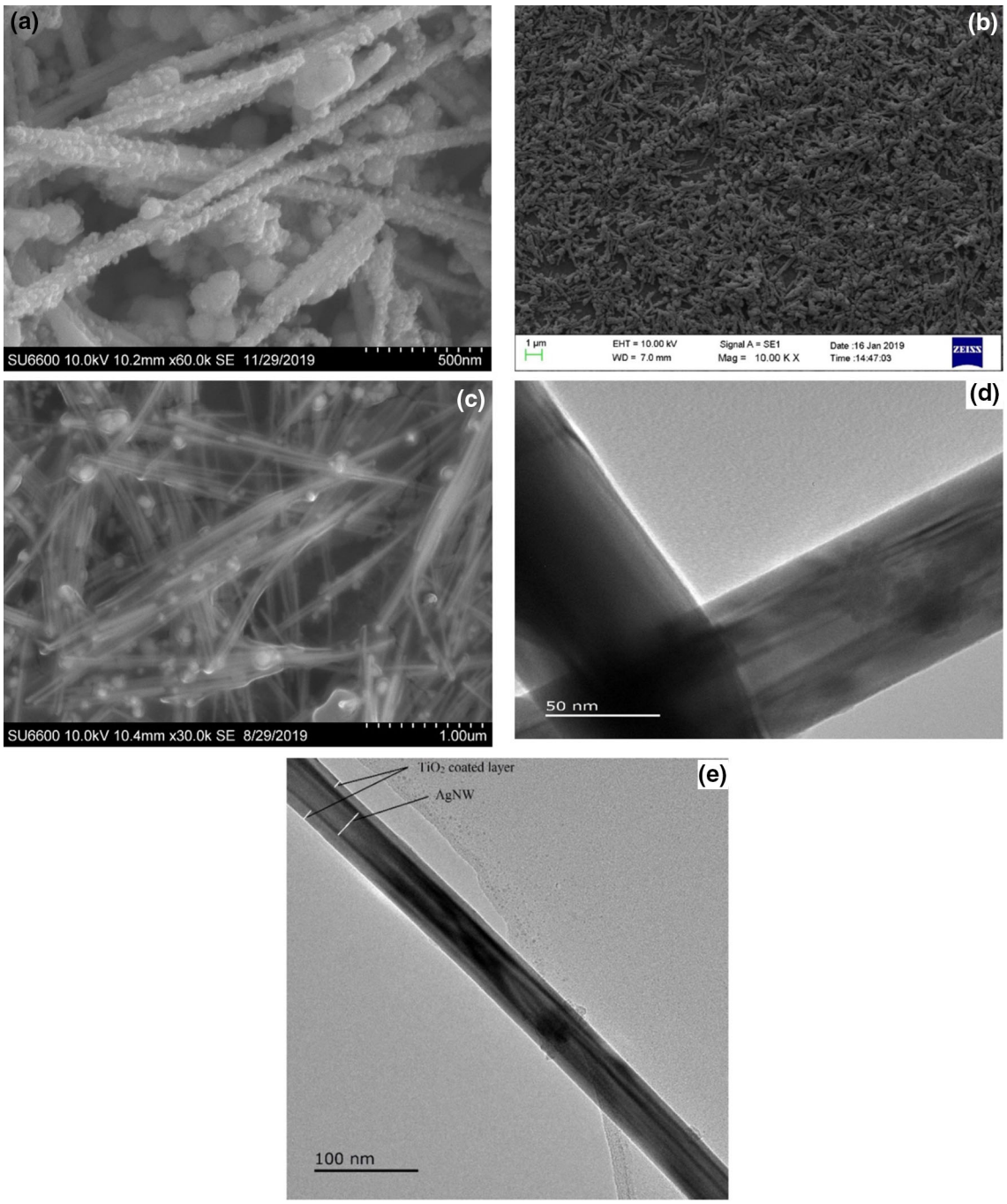

Figure 2. SEM images of (**a**) synthesized AgNWs@TiO_2 using 1.74 mM TBOT, (**b**) synthesized AgNWs@TiO_2 using 3.48 mM TBOT, (**c**) synthesized AgNWs@TiO_2 using 5.22 mM TBOT, (**d**) TEM image of synthesized AgNWs and (**e**) TEM image of synthesized AgNWs@TiO_2.

3.4 *UV–visible spectroscopy*

UV–visible analysis was carried out for 3 different samples as described below. Figure 3 shows UV–visible absorption spectra corresponding to (a) AgNWs and (b) AgNWs@TiO_2 samples. In the absorption spectrum of AgNWs, there are two absorption peaks visible at 350 and 390 nm. The shoulder peak around 350 nm corresponds to a longitudinal SPR mode as the bulk Ag [24,26]. Another explanation is the plane quadrupole mode of AgNWs [24]. The peak around 390 nm represents transverse plasmon resonance of AgNWs [24,27]. In spectrum (b) there is a peak redshift of 32 nm due to the TiO_2 core-shell and the longitude mode almost disappears because of the superior absorption of the TiO_2 core-shell. The shift in plasmon on encapsulation may be mainly due to the change in the

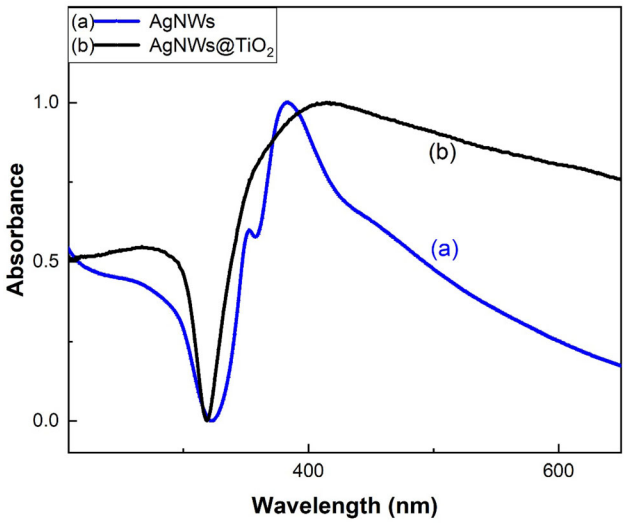

Figure 3. UV–visible spectra of (**a**) AgNWs and (**b**) TiO_2-coated AgNWs.

refractive index of the medium. Previous research shows that redshift tends to increase with increasing core-shell thickness [24,27]. In this case, core-shell thickness varies between 10 and 20 nm. This range was also confirmed by the SEM and TEM images.

3.5 *XRD analysis*

To obtain information on the crystalline structure and to confirm the presence of expected compounds, the AgNWs@TiO_2-incorporated photoanode powder sample was analysed using XRD. Figure 4 shows the XRD spectra of AgNWs@TiO_2-incorporated P25 mixture. Diffraction peaks in the spectrum corresponding to angles 38.56°, 44.68°, 64.80° and 77.06° were identified to be originating, respectively, from (111), (200), (220) and (311) planes of

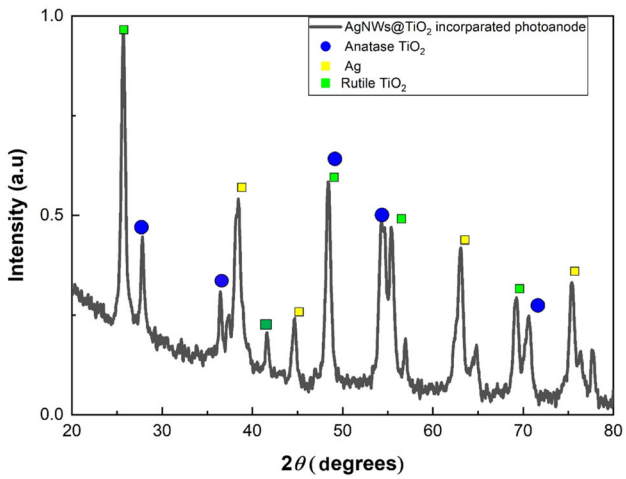

Figure 4. XRD analysis of AgNWs@TiO_2 and P25 NPs-incorporated photoanode.

the face-centred cubic Ag (JCPDS 04-0783). Furthermore, peaks visible at 28.19°, 37.8°, 46.60° and 50.85° can be assigned to (101), (004), (200) and (105) planes of anatase TiO_2, respectively (JCPDS 21-1272). The peak at 2θ = 37.80° could also be assigned to the TiO_2 plane as well, in addition to the Ag (111) plane. These peaks identified for Ag and TiO_2 in the sample XRD spectrum confirm the presence of both species in the AgNWs@TiO_2 powder sample [4,25].

The additional peaks located at 2θ = 27.3°,41.5°, 54.1° and 68.6° correspond to the rutile TiO_2 (110), (101), (211) and (301), respectively (JCPDS 21-1276), in the photoanode mixture, and are expected to occur at higher intensity as the commercially available P25 powder does contain both anatase and rutile phases of TiO_2. It can be confirmed that both anatase, rutile TiO_2 and Ag are present in the P25 + AgNWs@TiO_2 photoanode mixture [11,18]. How these two forms of TiO_2 NPs are attached to AgNWs will be explained later.

3.6 *Chemical identification of elements in the photoanode*

XPS analysis is highly sensitive to the surface chemical composition of a particular material. While giving an idea of the elements present, it also reveals information on the existence of different chemical statuses of the elements. Photoanodes were analysed using XPS. Figure 5a indicates the full XPS analysis of the photoanode. These spectra indicate the presence of all expected elements, such as; Silver (Ag), Titanium (Ti), Oxygen (O), and additionally Carbon (C). Figure 5a shows that the Ag 3d intensity is less than Ti because the amount of AgNWs@TiO_2 is very low compared to the P25 (TiO_2). However, Ti and O peaks have high intensities due to the higher amounts of TiO_2 existing in the photoanode. The existence of C can be explained as the residual C from the sample or adventitious hydrocarbon from the XPS instrument itself [4]. Figure 5b shows the high-resolution XPS spectra of the Ag 3d region. The spectrum consists of the two individual peaks at 373.7 and 367.6 eV [4], which can be attributed to Ag $3d_{5/2}$ and Ag $3d_{3/2}$ bands, respectively. The slitting of the Ag 3d doublet of 6.0 eV suggests the presence of zero valence silver instead of Ag^+ ions within the material. The shift of binding energy of Ag ($3d_{5/2}$) from 368.3 eV, which is the reported binding energy of Ag^0 ($3d_{5/2}$) to lower binding energy 367.5 eV, can be ascribed to the change in the chemical environment by functionalizing the surface of AgNWs using 2-mercaptoethanol [4,11,19–22].

The XPS peak at 462.9 eV corresponds to Ti $2p_{1/2}$, and 457.2 eV corresponds to Ti $2p_{3/2}$ in the Ti 2p region, figure 5c, in high-resolution XPS spectra of Ti 2p peaks. The slitting width between the two peaks was 5.64 eV, which represents the normal state of Ti^{4+} which belongs to the TiO_2 core shell [6]. The peak (C) at 472.1 eV represents the rutile Ti, which belong to P25 TiO_2 in the photoanode

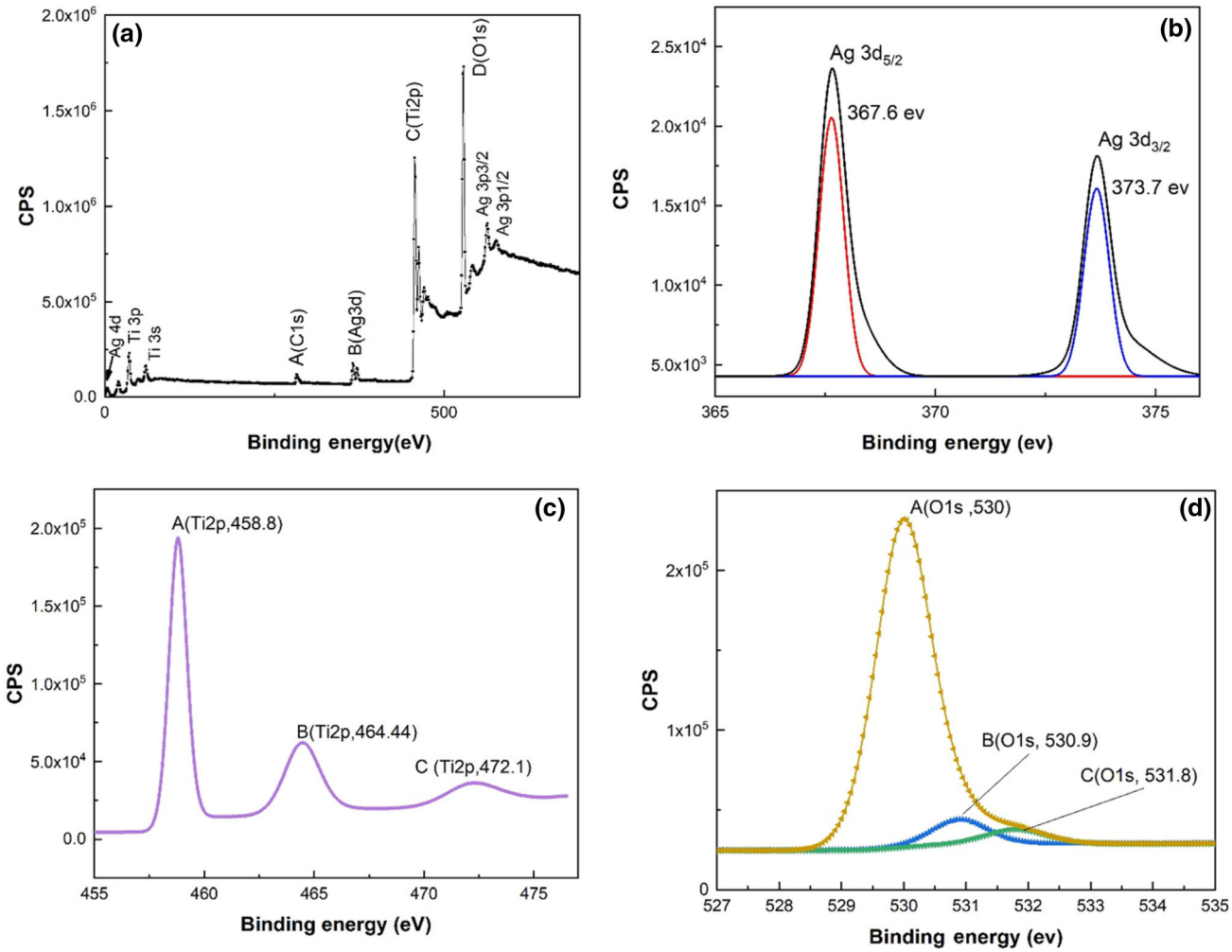

Figure 5. XPS serve of the photoanode, (**a**) elemental mapping of the photoanode, (**b**) XPS spectra of the Ag, (**c**) Ti, and (**d**) oxygen.

[4]. Figure 5d shows oxygen peaks at 530.0, 530.9 and 531.8 eV. These peaks represent the oxygen species of Ti–O, –OH and H_2O, respectively, where Ti–O is from the bonding of the TiO_2, H_2O is from the absorbed water molecules by the sample itself, and –OH is from 2-mercaptoethanol which was used as a chemical binder to form the AgNWs@TiO_2. XPS results can confirm the existence of the core-shell structure. In conclusion, XPS analysis confirms that TiO_2 was coated on the AgNWs and the –OH and shift in Ag^0 ($3d_{5/2}$) confirms the presence of 2-mercaptoethanol [4,11,21,24].

3.7 *DSSC photovoltaic performance*

In this study, two main DSSC configurations were fabricated and tested; (a) DSSC with single-layered photoanode and (b) tri-layered photoanode. A specific sequential process of layer by layer deposition followed by sintering, was used to obtain thicker and crack-free photoanodes. Single-layered DSSC was fabricated with AgNWs@TiO_2-incorporated photoanode on top of a P90 layer (P90/P25+Ag@TiO_2 NW), and a reference cell was fabricated with the photoanode configuration of P90/P25. To investigate DSSC performance with the AgNWs@TiO_2, a single-layer photoanode was prepared by varying the added amounts of AgNWs@TiO_2 as weight percentages compared to the weight of P25 powder used. The photovoltaic characteristics of AgNWs@TiO_2-incorporated single-layered photoanode-based DSSCs are tabulated in table 1. The measurements were conducted on eight samples for each batch and repeated three times (24 cells in total for one batch). According to table 1, the highest efficiency was observed for the 0.34 wt% AgNWs@TiO_2 added system.

The highest efficiency of 8.87% was observed for 0.34 wt% of AgNWs@TiO_2 added system with improved short circuit current (J_{sc}) compared to the reference DSSC without adding any AgNWs@TiO_2. The comparison of *J–V* curves for the prepared single-layered photoanode-based DSSCs are shown in figure 6a. The DSSC with the optimal performance (P90/P25+AgNWs@TiO_2 $_{(0.34\ wt\%)}$) was then modified to have triple layers in its photoanode,

Table 1. Photovoltaic parameters of prepared single-layered photoanode-based DSSCs with incorporation of different amounts of AgNWs@TiO_2.

Photoanode configuration	wt% of Ag@TiO_2NWs	V_{oc}, V	J_{sc}, mA cm^{-2}	Fill factor, %	Efficiency, %
P90/P25+AgNWs@TiO_2 (0.00 wt%)	0.00	0.74	14.3	60.8 ± 0.3	6.70 ± 0.02
P90/P25+AgNWs@TiO_2 (0.17 wt%)	0.17	0.67	17.3	57.4 ± 0.3	6.86 ± 0.05
P90/P25+AgNWs@TiO_2(0.34 wt%)	0.34	0.69	21.6	58.6 ± 0.5	8.87 ± 0.06
P90/P25+AgNWs@TiO_2(1.02 wt%)	1.02	0.69	20.6	54.4 ± 0.7	7.86 ± 0.03
P90/P25+AgNWs@TiO_2(1.36 wt%)	1.36	0.69	17.0	63.1 ± 0.3	7.62±0.08

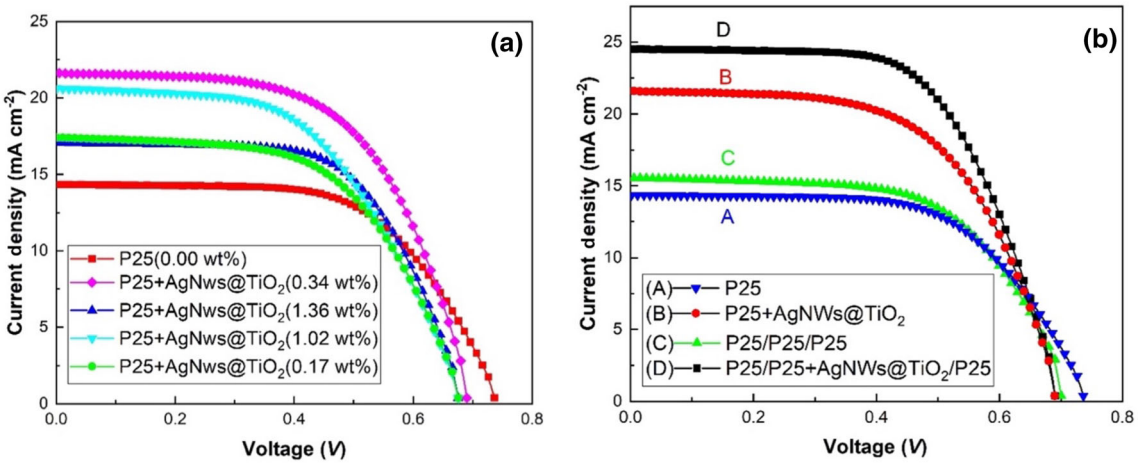

Figure 6. (**a**) The *J–V* characteristics of single-layered DSSC of 6 different AgNWs@TiO_2 concentrations. (**b**) *J–V* characteristics of two single-layered DSSC and two different tri-layered DSSCs.

with the composition of P25/P25+AgNWs@TiO_2/P25. A reference tri-layered cell was also constructed with the photoanode composition of P25/P25/P25 and compared with the AgNWs@TiO_2 added system. *J–V* curves of single-layered and triple-layered DSSCs are illustrated in figure 6b, and the corresponding photovoltaic parameters are tabulated in table 2, which is highest recorded PCE out of 3 DSSC. All the *J–V* measurements were taken under simulated sunlight illuminated at 100 mW cm^{-2} (AM 1.5).

According to table 2, the photovoltaic parameters of triple-layer DSSCs are improved compared to single-layer photoanodes-based DSSCs. It can be seen that J_{sc} is mainly responsible for the enhancement of the DSSC in AgNWs@TiO_2 added systems (table 2B and D). But the decrease of open-circuit voltage (V_{oc}) values relative to the reference DSSCs may be due to an increase of recombination by adding AgNWs@TiO_2 to the system. This can be a result of the higher recombination probability of the

Table 2. Comparison of photovoltaic parameters of the DSSCs with single-layer, bilayer and tri-layer photoanodes with different amounts of AgNWs@TiO_2.

Photoanode configuration	V_{oc}, V	J_{sc}, mA cm^{-2}	Fill factor, %	Efficiency, %	References
(A) P90/P25	0.74	14.3	60.8 ± 0.3	6.70 ± 0.02	This study
(B) P90/P25+Ag@TiO_2 $NWs_{(0.34\ wt\%)}$	0.69	21.6	58.6 ± 0.5	8.87 ± 0.06	This study
(C) P90/P25/P25/P25	0.70	15.7	62.9 ± 0.4	7.04 ± 0.07	This study
(D) P90/P25/P25+ Ag@TiO_2 $NWs_{(0.34\ wt\%)}$/P25	0.69	24.5	61.3 ± 0.5	10.5 ± 0.08	This study
P90/P25/(P25+TiO_2NF+AgNW)/P25	67.6	14.3	0.727	9.74	[5]
P90/P25+Ag/AgBr/TiO_2	63.0	18.78	0.712	8.46	[35]
P25/P25+$AgNW_{(3\ wt\%)}$	61.01	13.01	0.741	5.88	[36]
P90/P25+$AgNW_{(0.9\ wt\%)}$	0.718	18.03	65.26	9.41	[6]

tri-layered photoanode. Higher dye absorption creates more excited electrons resulting in a higher J_{sc} leading to a higher PCE in tri-layered reference cells. The efficiency enhancement of AgNWs@TiO_2-incorporated single-layered DSSC compared to the single-layered reference cell is 32.3%.

$$V_{oc} = \frac{nkT}{q}\left(\ln\left(\frac{I_L}{I_0}+1\right)\right) \quad (2)$$

According to equation (2), where I_L is the light generated current, I_o reverse saturation current, n is the ideality factor (normally denoted as 1), and kT/q is the thermal voltage, the V_{oc} is open-circuit voltage which depends on the saturation current I_0 and the light generated current I_L of the solar cell. Accordingly, the reduction of V_{oc} might be due to increased charge transportation in the presence of AgNWs, which can increase the recombination current (I_0). The increase in J_{sc} is higher than the decrease in V_{oc}. The reason behind the higher J_{sc} in the DSSC with AgNWs@TiO_2-incorporated photoanode can be the AgNWs, which provide a direct pathway for excited electrons from dye to current collector (FTO) [5–11,18–24]. Further, the TiO_2 core-shell in AgNWs introduces multiple light scattering pathways inside the photoanode, and hence increasing light absorption results in an increase in light-generated J_{sc}. This effect is further explained in the IPCE analysis.

In the tri-layered photoanode configuration, there is a significant 49.6% increase in PCE of AgNWs@TiO_2-incorporated DSSC compared to that of reference tri-layered DSSC. We can observe that just like in the single-layered DSSC, V_{oc} is decreased but J_{sc} is increased due to the scattering effect of the coated TiO_2 core-shell and conduction properties of AgNWs, which will be described in detail at IPCE analysis. AgNWs have been proven to be a good transportation medium for the excited electron [5–10]. The increment in PCE of tri-layer photoanode-based DSSCs are due to high dye adsorption in tri-layer TiO_2 structure and the plasmonic effect of the AgNWs. The local plasmonics effect of Ag causes a high impact on the PCE of DSSC. Additionally, AgNWs provide a direct pathway for excited electron which will increase the J_{sc} [5–11,18–24].

The presence of the TiO_2 in the core-shell structure is expected to act as a protective layer around the AgNWs, preventing any electrolyte reactions with the AgNWs.

The introduction of additional layers has increased the efficiency from 6.70 to 7.04, table 2A and C. Additional layers of (C) increase the dye absorption hence J_{sc} has increased. The fill factor has increased due to higher dye absorption, as in table 3 [6].

The cross-section of the tri-layered structure was analysed using SEM. Figure 7 shows the SEM image of the two tri-layered photoanode. Each layer thickness was mentioned on the image with a total thickness of 50.3 μm. And for reference photoanode total thickness is 50.9 μm. So the thickness of two different photoanodes are same, which leads to PCE enhancement as only cause is due to the presence of AgNWs@TiO_2.

3.8 *IPCE analysis*

IPCE measurements explain the efficiency in the conversion of light photons to electrons at different wavelengths. The IPCE variations were taken for these 4 types of DSSCs; a, b, c and d, are elaborated in figure 8.

The area under an IPCE curve is directly proportional to the photocurrent density of the DSSC. Thus, it could be seen that tri-layered DSSCs show a much higher photocurrent than the single-layered DSSCs. This could be due to the higher dye absorption by the increased amounts of TiO_2 in the tri-layered DSSCs' photoanodes. The higher the amount of dye loaded onto the semiconducting matrix, the higher the number of generated photoelectrons, hence the higher photocurrent [5,22,23]. The comparison between IPCE curves (a) and (c), and also (b) and (d), clearly shows the advantageous effect that the increased thickness of a photoanode has on converting incident light to electrons.

By comparing, figure 8, curves (a), (b) and also (c), (d), the effect of AgNWs@TiO_2 in the photoanode of single-layered DSSC can be studied. The LSPR effect of silver nanostructures can be observed at 350 and 390 nm (figure 3a). However, as described in UV–visible analysis, by adding TiO_2 core-shell 350 nm is disappeared, as well as there have been a red-shift. At last, the current structure's plasmonic effect is around 420 nm (figure 3c). A considerable number of research articles can be cited to show the LSPR effect of silver nanostructures [5–7,20,28–34]. It could be seen that both single- and tri-layered DSSCs incorporated with AgNWs@TiO_2 show increased photocurrents with respect to each of their reference cells at around 420 nm. The IPCE behaviour in the curve

Table 3. Amount of dye absorption of DSSC with single-layered and tri-layered with and without AgNWs@TiO_2.

Cell type	Amount of dye absorbance (reference) ($\times 10^{-7}$ mol)	Amount of dye absorbance (AgNWs@TiO_2-incorporated cell) ($\times 10^{-7}$ mol)
Single-layer photoanode	1.33	2.02
Tri-layer photoanode	2.88	4.15

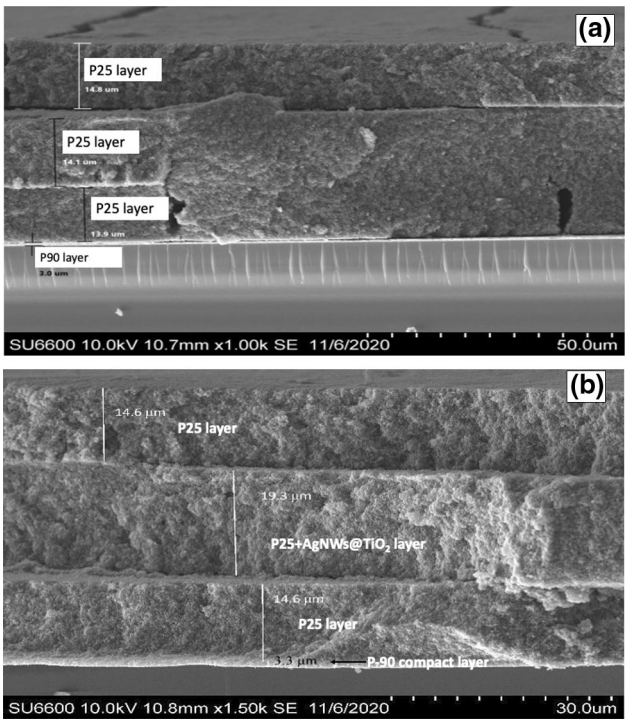

Figure 7. Cross-sectional SEM image of the tri-layered photoanode. (**a**) Tri-layered reference photoanode and (**b**) AgNWs@TiO_2-incorporated try-layered photoanode.

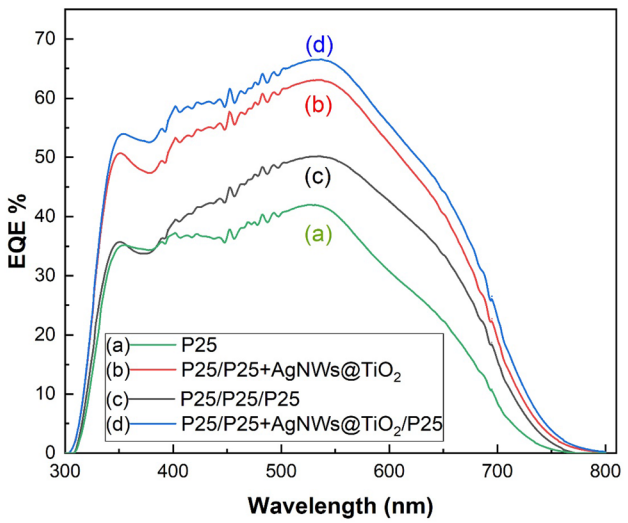

Figure 8. IPCE spectra of two single-layered DSSCs and two tri-layered DSSCs. (**a**) Single-cell DSSC (P90/P25), (**b**) single-layered DSSC (P90/(P25+AgNWs@TiO_2)), (**c**) tri-layered (P90/P25/P25/P25) and (**d**) tri-layered (P90/P25/(P25+AgNWs@TiO_2)/P25).

(b) supports the increase in J_{sc} in AgNWs@TiO_2-incorporated single-layered DSSC with respect to its reference cell (c) at 420 nm. It is evident that this enhancement is caused by the wavelength-dependent plasmon effect of AgNWs and also due to better electron-conducting pathways created by the nanowires inside the semiconductor. SPR effect rendered from AgNWs generates localized electromagnetic fields, which efficiently accelerates the excitation and electron injection from the dye [4,5]. This might be the reason for the increase in peak IPCE values of single-layered and tri-layered DSSCs at 420 nm with AgNWs@TiO_2 in comparison to their reference cells. Also, the SPR effect results in the scattering of the incident light, consequently increasing a photon's optical path length, thus increasing light-harvesting efficiency.

At 535 nm, there is incensement of IPCE for figure 8, curve (b) with respect to the reference curve (a) which is due to the higher dye absorbance of core-shell structure of AgNWs. The same results can be observed from the tri-layered reference (figure 8, curve (c)) cell and AgNWs@TiO_2-incorporated cell (curve (d)). In comparison of curves (a) and (c), incensement of thickness, higher photocurrent are also expected. This can be expected because when thickness is higher, dye absorption definitely increases. This dye absorption can be confirmed by referring table 3 also. It is clearly shown that the dye absorption amounts, after incorporating AgNWs@TiO_2, have increased because TiO_2 core-shell structure that have anatase from TiO_2 also absorb the dye. And after increasing thickness of photoanode's, dye absorption also has increased.

Tri-layered DSSC with AgNWs@TiO_2 in the photoanode benefits from all above-mentioned factors; increased photoanode thickness, properties given by SPR effect, and good conducting pathways due to TiO_2-coated AgNWs, thus shows the highest peak IPCE curve. IPCE mainly depends on the light-harvesting efficiency, the efficiency of electron injection from the excited dye molecule to the TiO_2 electrode, and the electron collection efficiency at the anode. The increased IPCE of AgNW@TiO_2-incorporated tri-layered cells can be attributed to the increase in all these parameters and can be directly used to explain the high J_{sc} value obtained for that particular solar cell [5–7,11,18–24].

In general, it can be explained that, nanostructure with diameter more than 90 nm are helping scattering effect and diameter less than 90 nm are very strong light absorbances [30]. Our SEM and TEM images show that, if the diameter of synthesized AgNWs are in the range of 40–100 nm, then it can be both scattering and absorbance, hence the higher J_{sc} as a result of that, higher PCE can be expected.

3.9 *EIS measurements*

EIS measurements are used to identify the electronic and ionic transport mechanisms of the DSSC. Nyquist plots were obtained for; (A) P25/P25/P25, (B) P25/AgNWs@TiO_2+P25/P25, tri-layered DSSCs, shown in figure 9a Nyquist plots for tri-layered DSSCs which are reference and AgNWs@TiO_2 incorporated DSSCs. Two semi-circles were seen in each plot. The larger semicircle in

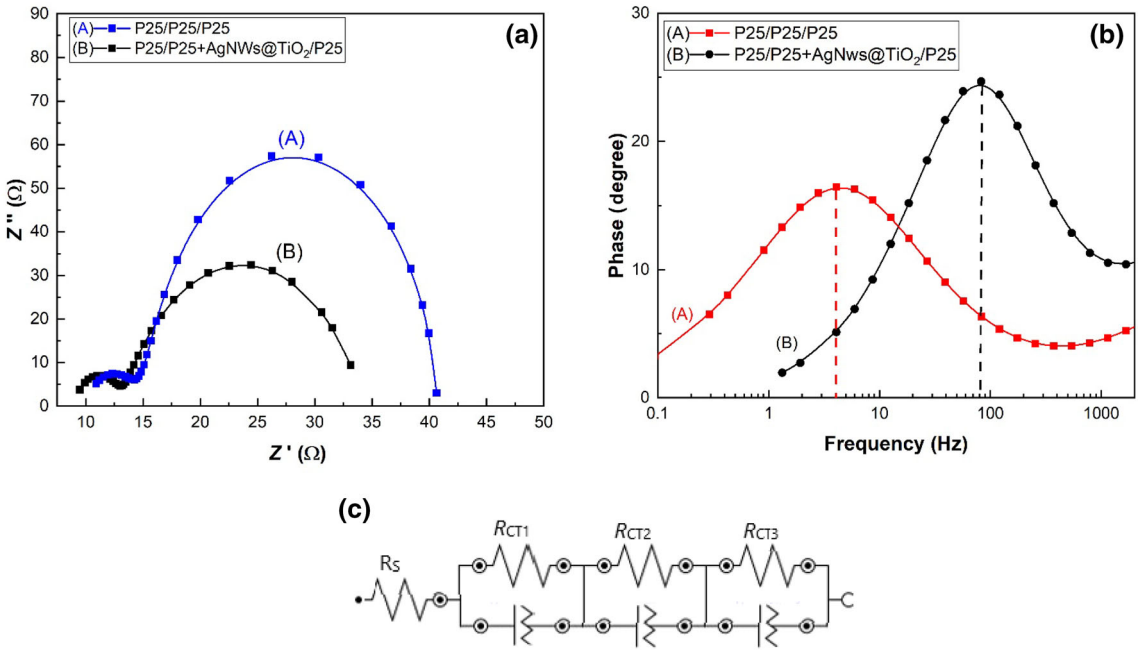

Figure 9. (**a**) EIS graph of tri-layered DSSC (equivalent circuit data graph as a line connected graph) and (**b**) Bode phase graph of tri-layered DSSC. (**c**) Equivalent circuit to graph (**a**).

the low-frequency region represents the charge transfer resistance at dye-attached TiO_2/electrolyte interface (R_{CT2}). The smaller semicircle represents charge transfer resistance at the Pt counter electrode/electrolyte interface (R_{CT1}) [2,5]. The impedance data extracted using an equivalent circuit is shown in figure 9c. The maximum frequency (f_{max}) can be observed from Bode phase graphs in figure 9b and hence electron lifetime (τ_e) can be calculated through equation (3) [23]. These calculated values and the extracted impedance data are shown in table 4.

$$\tau_e = \frac{1}{2\pi f_{max}} \tag{3}$$

R_{CT1} decreases with respect to the reference cell. This implies an increase in oxidation and redox mediator at the counter electrode. AgNWs@TiO_2-incorporated DSSCs have decreased the R_{CT2} with respect to their respective reference cells. This indicates AgNWs charge transfer mechanism across the anode and electrolyte because AgNWs are better electron conductors. The redox couple reaction releases more electrons, so this explains electrons have reached the oxidized dye mole more easily [4].

AgNWs@TiO_2-incorporated tri-layered DSSC have the lowest electron lifetime than reference DSSC. It is possible because, in this photoanode, lower electron lifetime suggests faster the recombination of photoelectrons. Therefore, the AgNWs@TiO_2-incorporated cell can increase non-radioactive recombination with dye or electrolyte. This leads to reduced number of electrons gather at electrode, hence reduction of V_{oc} might be related to the increased electron recombination. However, an increase in J_{sc} suppresses the outcome of the DSSC performance.

3.10 *Thermal stability after coating TiO_2*

Figure 10a shows that the SEM images of heat treatment at 450°C silver nanowires remain intact in the presence of TiO_2 core-shell structure, which means TiO_2 core-shell structure acts as a protective shield around the AgNWs. However, heat treatment at 650°C (figure 10b) shows no trace of AgNWs. This means that at 450°C, the AgNWs@TiO_2 remains intact when fabricating the DSSC, so during the DSSC characterization, the AgNWs structure

Table 4. Charge transfer resistances extracted from the Nyquist plots and electron lifetimes extracted from the Bode phase plots.

Cell type	R_{CT1}, Ohms	R_{CT2}, Ohms	J_{sc} mA cm^{-2}	Frequency (f_{max}) Hz	Electron lifetime τ_e, (ms)	Efficiency %
P25/P25/P25	24.3	4.42	15.7	4.09	39.1	7.04 ± 0.07
P25/P25+AgNWs@TiO_2/P25	4.22	2.92	24.5	82.8	1.92	10.5 ± 0.08

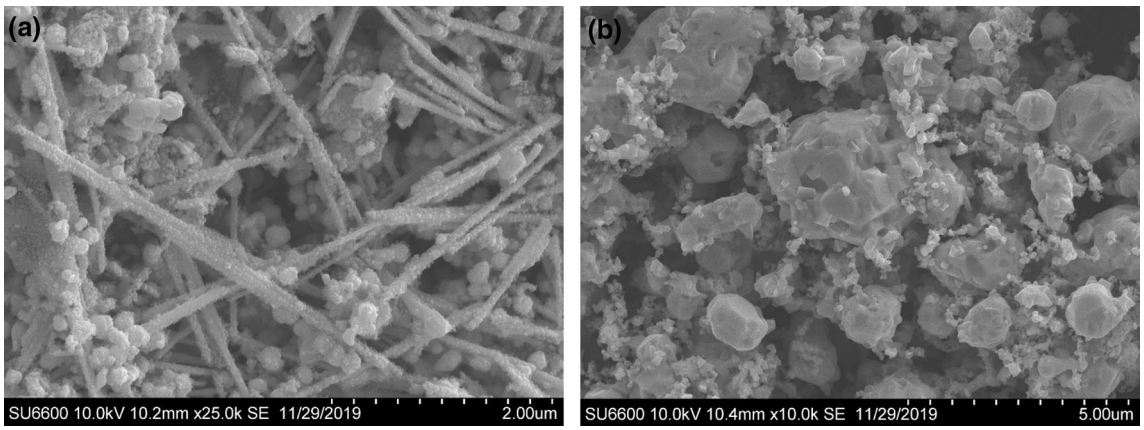

Figure 10. SEM images of AgNWs@TiO_2 for different heat treatments. (**a**) Heat treatment at 450°C and (**b**) 650°C.

is present as we expected. Similar work has been conducted on this study before [24].

4. Conclusion

The effect of using a single-layered and tri-layered photoanodes fabricated with AgNWs@TiO_2 core-shell structure was studied by applying it in DSSCs. The tri-layered DSSC which was made as AgNWs@TiO_2 were incorporated into the middle layer of DSSC in a sandwich between two P25 layers. First, the AgNWs@TiO_2 concentration in the P25 layer of the single-layered structure was optimized with respect to the reference cell. The PCE for a DSSC with single-layered TiO_2 photoanode increased from 6.7 to 8.8% due to AgNW@TiO_2 core-shell-structured photoanode, reflecting a 32.3% enhancement. The PCE for a DSSC with tri-layered AgNW@TiO_2 core-shell-structured photoanode was 10.5%, showing an impressive enhancement of 49.6% compared to the DSSC with pure tri-layered TiO_2 photoanode. The improvement of DSSC has been proven using the *J–V* characteristics, IPCE, EIS measurements and Bode phase graphs. The increase of the J_{sc} could be explained by, (i) plasmonic effect facilitating the photoelectron generation in the core-shell structure of AgNWs@TiO_2, increasing charge recombination, improving the electron transfer rate and electrons lifetime, and giving a direct pathway for transport of excited electrons. (ii) The dynamic light scattering of the TiO_2 core-shell and its higher dye absorption by increasing the effective surface area and enhancing light absorption due to LSPR effect of the AgNWs.

Acknowledgement

HKHD Kankanamge would like to thank Dr C A Thotawatthage, Dr T Jaseetharan and Mrs Imali Madikasekara of the National Institute of Fundamental Studies (NIFS) for their support during the experimentation stage. H C S Perera gratefully acknowledges the financial support provided by the National Science Foundation (NSF) under Grant No. RG/2018/BS/01.

Reference

[1] O'Regan B and Grätzel M 1991 *Nature* **353** 737
[2] Dissanayake M A K L, Kumari J M K W, Senadeera G K R and Thotawatthage C A 2016 *J. Appl. Electrochem.* **46** 47
[3] Jang Y H, Jang Y J, Kochuveedu S T, Byun M, Lin Z, Kim D H *et al* 2014 *Nanoscale* **6** 1823
[4] Jang I, Kang T, Cho W, Kang Y S, Oh S-G, Im S S *et al* 2015 *J. Phys. Chem. Solids* **86** 122
[5] Kumari M G C M, Perera C S, Dassanayake B S, Dissanayake M A K L and Senadeera G K R 2019 *Electrochim. Acta* **298** 330
[6] Chandrasekhar P S, Elbohy H, Vaggensmith B, Dubey A, Reza K M, Komarala V K *et al* 2017 Mater. Today. *Energy* **5** 237
[7] Garmaroudi Z A and Mohammadi M R 2016 *J. Am. Ceram. Soc.* **99** 167
[8] Stojanovic N, Maithripala D H S, Berg J M and Holtz M 2010 *Phys. Rev. B - Condens. Matter Mater. Phys.* **82** 1
[9] Kelly K L, Coronado E, Zhao L L and Schatz G C 2003 *J. Phys. Chem. B* **107** 668
[10] Hutter E and Fendler J H 2004 *Adv. Mater.* **16** 1685
[11] Ma C, Wang X, Luo H and Zhang D 2017 *J. Mater. Sci. Mater. Electron* **28** 10715
[12] Zhang Q and Cao G 2011 *Nano Today* **6** 91
[13] Barnes W L, Dereux A and Ebbesen T W 2003 *Nature* **424** 824
[14] Qingsong J, Jian G, Hong T, Guojia F, Helin W, Lin Y *et al* 2014 *Mater. Lett.* **134** 16
[15] Wen C, Ishikawa K, Kishima M and Yamada K 2000 *Sol. Energy Mater. Sol Cells* **61** 339
[16] Jeong N C, Prasittichai C and Hupp J T 2011 *Langmuir* **27** 14609
[17] Fan Y H, Ho C Y and Chang Y J 2017 *Scanning* **2017** 1
[18] Du P, Cao Y, Li D, Liu Z, Kong X, Sun Z *et al* 2013 *RSC Adv.* **3** 6016

[19] Chen T-Y, Fan C M, Wu J Y and Lin T L 2009 *J. Chinese Chem. Soc.* **56** 1244
[20] Cheng Y, Youhong T, Zijin S, Zhexu Z and Cheng F 2015 *J. Mater. Sci. Technol.* **31** 16
[21] Cheng B, Le Y and Yu J 2010 *J. Hazard Mater.* **177** 971
[22] Dissanayakea M A K L, Jaseetharana T, Senadeera G K R, Mellander B-E, Albinson I, Furlanie M *et al* 2019 *J. Solid State Electrochem.* **23** 1787
[23] Dissanayake M A K L, Sarangika H N M, Senadeera G K R, Divarathna H K D W M N R and Ekanayake E M P C 2017 *J. Appl. Electrochem.* **47** 1239
[24] Ramasamy P, Seo D-M, Kim S-H and Kim J 2012 *J. Mater. Chem.* **22** 11651
[25] Johan M R, Aznan N A K, Yee S T, HongHo I, Ooi S, Singho N D *et al* 2014 *J. Nanomater.* **2014** 1
[26] Sun Y, Gates B, Mayers B and Xia Y 2002 *Nano Lett.* **2** 165
[27] Wang Z, Liu J, Chen X, Wan J and Qian Y 2005 *Chem. - A Eur. J.* **11** 160
[28] Gangishetty M K, Lee K E, Scott R W J and Kelly T L 2013 *ACS Appl. Mater. Interfaces* **5** 11044
[29] Ferry V E, Munday J N and Atwater H A 2010 *Adv. Mater.* **22** 4794
[30] Erwin W R, Zarick H F, Talbert E M and Bardhan R 2016 *Energy Environ. Sci.* **9** 1577
[31] Schuck P J 2013 *Nat. Nanotechnol.* **8** 799
[32] Schaadt D M, Feng B and Yu E T 2005 *Appl. Phys. Lett.* **86** 1
[33] Marchuk K and Willets K A 2014 *Chem. Phys.* **445** 95
[34] Ihara M, Tanaka K, Sakaki K, Honma I and Yamada K 1997 *J. Phys. Chem. B* **101** 5153
[35] Madigasekara I, Perera C S, Kumari J M K W, Senadeera G K R and Dissanayakea M A K L 2021 *Sol. Energy* **230** 59
[36] Chou J C, Lin Y C, Lai C H, Kuo P Y, Nien Y H, Chang J X *et al* 2021 *IEEE J. Electron Devices Soc.* **9** 250